Title: Structural, lattice vibrational, optical and microwave dielectric studies on $Ca_{1-x}Sr_xMoO_4$ ceramics with scheelite structure

Author: S.D. Ramarao S.Roopas Kiran V.R.K. Murthy

PII: S0025-5408(14)00249-9
DOI: http://dx.doi.org/doi:10.1016/j.materresbull.2014.04.064
Reference: MRB 7436

To appear in: *MRB*

Received date: 3-9-2013
Revised date: 10-3-2014
Accepted date: 24-4-2014

Please cite this article as: S.D.Ramarao, S.Roopas Kiran, V.R.K.Murthy, Structural, lattice vibrational, optical and microwave dielectric studies on Ca1-xSrxMoO4 ceramics with scheelite structure, Materials Research Bulletin http://dx.doi.org/10.1016/j.materresbull.2014.04.064

Structural, lattice vibrational, optical and microwave dielectric studies on $Ca_{1-x}Sr_xMoO_4$ ceramics with scheelite structure

S.D. Ramarao[1], S. Roopas Kiran[2], V.R.K. Murthy[1,*]

[1]*Microwave laboratory, Department of Physics, Indian Institute of Technology Madras, Chennai 600 036, India.*
[2]*INFN, Sezione di Padova, Via Marzolo 8, 35131 Padova, Italy.*

*Corresponding author: Telephone +91-44-22574859; Fax: +91-44-22570545

E-mail: vrkm@iitm.ac.in

Graphical abstract

Highlights

- Microwave dielectric properties of scheelite $Ca_{1-x}Sr_xMoO_4$ ceramics are studied.
- ε_r correlated with unit cell volume in contrast to polarizability.
- Q×*f* of these compositions explained with Mo-O bond strength.
- Interesting correlation between τ_f and Raman shift of A_{1g} mode is observed.
- Non monotonic variation in band gap is observed and fitted with bowing equation.

Abstract:

Structural, optical and microwave dielectric properties of $Ca_{1-x}Sr_xMoO_4$ (x= 0.0, 0.2, 0.4, 0.6, 0.8 and 1.0) compositions were studied with help of Rietveld refinement and Raman spectroscopy measurements. All these compositions were prepared by solid state reaction method and observed to possess tetragonal scheelite structure with $I4_1/a$ space group. Microwave dielectric properties such as dielectric constant (ε_r), quality factor (Q×*f*) and temperature coefficient of resonant frequency (τ_f) were measured using Hakki-Coleman method, Reflection technique and invar cavity attached to hot plate respectively. ε_r, (Q×*f*) and

τ_f are correlated with molar volume (V_m), Mo-O bond strength and Raman shift of A_{1g} mode respectively. All these compounds show good microwave dielectric properties (ε_r = 6.7–9.6, $Q \times f$ = 35000–52000 GHz and τ_f = -28 to -17 ppm/^oC). Band gap of these compositions was observed in the range 3.3–3.5 eV and variation in band gap was fitted with Bowing equation.

.

Keywords: Ceramics; X-ray diffraction; Raman spectroscopy; dielectric properties; optical properties.

1. Introduction

Dielectric ceramics such as Dielectric Resonators (DR) play an important role in the rapid growth of mobile, satellite and radar communication [1, 2]. These dielectric resonators should possess high dielectric constant (ε_r>20) for miniaturization of electronic components, low dielectric loss (high Quality factor) for enhancing the selectivity of particular frequency and near-zero temperature coefficient of resonant frequency (τ_f). Perovskites (ABO_3) and complex perovskites ($ABB'O_3$) were extensively studied for microwave dielectric resonator applications with substitution of different cations at A- and B-sites [3-5].

Recently researchers focused on the microwave dielectric properties of $A^{2+}B^{6+}O_4$ compositions with scheelite and wolframite structures. Depending on the ionic radius of A-site cation, the $A^{2+}B^{6+}O_4$ (A: Ca, Sr, Ba; B: Mo, W) compounds exhibit scheelite structure with $I4_1/a$ space group and wolframite structure with P2/c space group [6, 7]. In scheelite structure A- and B-site cations possess coordination number eight and four respectively whereas in wolframite structure both cations possess six coordination numbers. Numerous investigations were reported on scheelite compounds for cathode material in solid oxide fuel cells [8], photo catalytic [9] and photoluminescent materials [10, 11]. Vibrational spectra were also reported by many researchers with complete assignment of Raman and IR modes [12-14]. Recently these $A^{2+}B^{6+}O_4$ compounds gained much attention in LTCC technology

because of their lower sintering temperatures (≤ 1200 ^{o}C) and flexibility for the substitution of different elements at A- and B-site to obtain optimum microwave dielectric properties. The compounds with lower sintering temperature and good microwave dielectric properties was reported by Zhou *et al.* in $xBi(Fe_{1/3}Mo_{2/3})O_4$–(1 x)$BiVO_4$ system in which the Raman and Infrared spectroscopy were implied to understand the phase transition mechanism. With increasing the x value from 0 to 0.1 the phase transition temperature observed to decrease from 255 ^{o}C to -9 ^{o}C and obtained good microwave dielectric properties even at lower sintering temperatures [15]. Zhou *et al.* reported the ultralow sintering temperature (around 620 ^{o}C) compound with higher dielectric constant and lower τ_f values by substituting Li^{1+} and Bi^{3+} at A-site of $A(W,Mo)O_4$ compounds [16].

Yoon *et al.* reported the structure and microwave dielectric properties of AWO_4 compounds based on the ionic radius of A-site cation and observed that the compounds with lower ionic radius of cations at A-site possessed higher quality factor [17]. Puller *et al.* explained the microwave dielectric properties of AWO_4 (A= Mg, Zn, Ni and Co) compounds with extrinsic parameter such as density [18]. Kim *et al.* studied the microwave dielectric characteristics of (1-x)$CaWO_4$ – x$LaNbO_4$ compounds and observed an interesting correlation between the quality factor and atomic packing fraction [19]. Choi *et al.* calculated the polarizability of Mo in $AMoO_4$ (A= Ca, Sr, Ba, Mg, Zn, and Mg) compounds using least square refinement in conjunction with the Clausius–Mosotti relation and correlated τ_f with the unit cell volume of [7]. Kim *et al.* correlated the quality factor, τ_f of scheelite $A^{2+}B^{6+}O_4$ compounds with the packing fraction and oxygen bond valence (V_O) respectively [20]. A similar correlation was also observed by Liao *et al.* in $ZnTiNbTaO_8$ compound [21]. However, a slight contradictory result was observed by Kim *et al.* in the case of $NiWO_4$ compound and correlated the lower quality factor of $NiWO_4$ with presence of unpaired 3d electrons in Ni^{2+} even though $NiWO_4$ has higher packing fraction [22]. Zhou *et al.* reported

that the dielectric constant of scheelites got enhanced with substitution of Bi^{+3} and alkali earth elements at A-site of $A^{2+}B^{6+}O_4$ compounds [23, 24]. Hence the microwave dielectric properties of $A^{2+}B^{6+}O_4$ compounds would depend on the structural parameters such as packing fraction [20] and bonding characteristics [25].

In the present paper we report the structural, lattice vibrational, microwave dielectric and optical properties of $Ca_{1-x}Sr_xMoO_4$ (x = 0.0, 0.2, 0.4, 0.6, 0.8 and 1.0) compounds. Rietveld refinement was performed on all these compositions to study phase purity of these compositions. Lattice vibrational characteristics such as Raman shift of A_{1g} mode of these compositions were analyzed from the Raman spectra. Microwave dielectric properties of these compounds are correlated with lattice vibrational characteristics in conjunction with structural parameters. The variation in the band gap of these compositions is fitted with Bowing equation.

2. Experimental Procedure

$Ca_{1-x}Sr_xMoO_4$ (x= 0.0, 0.2, 0.4, 0.6, 0.8 and 1.0) compounds were synthesized by conventional solid state reaction method. Proportionate amounts of starting reagents $CaCO_3$ (99.95%), $SrCO_3$ (99.9%) and MoO_3 (99.95%) (Alfa Aesar, USA) were mixed and hand ground in an agate mortar with distilled water medium for 2 h. All these compounds were calcined at 900 ^oC for 3 h. Cylindrical pellets of about 8 mm diameter and 7 mm thickness were prepared using uniaxial hydraulic press by adding 3 wt% PVA to the calcined powders. All these compacted pellets were sintered in temperature range 1100 – 1300 ^oC for 3 h.

Phase identification was done by obtaining powder diffraction data of all the sintered samples using Philips PANAlytical X'pert Pro X-ray diffractometer with X'Celerator detector and Cu K_α radiation at acceleration conditions of 40 kV and 30 mA. The incident and receiving soller slits of 0.02 rad and the divergent slit of 1^o were used and data was collected in the range of 10–120^o with a scan step of 0.017^o. Rietveld refinement was performed using

GSAS suite with EXPGUI to obtain the cation–oxygen bond lengths in $Ca_{1-x}Sr_xMoO_4$ (x= 0.0, 0.2, 0.4, 0.6, 0.8 and 1.0) compounds [26, 27]. Raman spectra of polished and thermally etched samples were collected using Horiba Jobin Yvon HR800 UV Raman spectrometer equipped with Peltier-cooled charge-coupled device detector. He-Ne laser source (λ=632.8 nm) was used for the measurement and the laser output power measured at the sample was about 3 mW. The optical band gap of these compounds was calculated from the optical absorption spectra using UV-Vis dual beam spectrophotometer (Jasco V-570) at room temperature.

The bulk densities of all these samples were measured using the Archimedes technique. Microstructures of polished and thermally etched samples were observed by FEI Quanta 400 high resolution Scanning Electron Microscopy. Microwave dielectric characterization was done using Vector Network Analyzer (Agilent PNA-L N5230C). Dielectric constant was obtained by Hakki-Coleman method [28]. Quality factor was measured by reflection technique with gold coated copper cavity. Temperature coefficient of resonant frequency (TCF) measured in the temperature range of 25-85 ^oC using an invar cavity. The TCF was calculated by the following formula

$$\tau_f = \frac{f_{85} - f_{25}}{f_{25} \times (85 - 25)} \text{ ppm/}^oC \quad (1)$$

where f_{85} and f_{25} are the resonant frequencies at 85^{o}C and 25^{o}C respectively.

3. Results and Discussion

3.1 Structure and Lattice Vibrational Analysis

The room temperature XRD patterns of $Ca_{1-x}Sr_xMoO_4$ (x= 0.0, 0.2, 0.4, 0.6, 0.8 and 1.0) are shown in the Fig. 1. It is clearly understood from this figure that, all these compositions form a solid solution with tetragonal scheelite structure and $I4_1/a$ (No: 88, Z=4) space group. All these patterns were indexed with JCPDS file number 29-351 and 30-1287. As

the ionic radius of Sr^{2+} (1.26 Å) is greater than Ca^{2+} (1.12 Å) [29], with substitution of Sr^{2+} in place of Ca^{2+} the lattice parameters get increased which inturn increases the unit cell volume. Correspondingly all the XRD reflections are observed to shift to lower angle side as shown in Fig. 1.

Rietveld refinement was performed on all these compositions to examine the variation in bond length of cation–oxygen bonds and nature of bonding. The initial parameters for the refinement of $CaMoO_4$ system was taken from Daturi *et al.* [6]. The refined plot for $Ca_{0.6}Sr_{0.4}MoO_4$ composition is shown in Fig. 2 as a representative. All the refinement parameters such as fractional atomic coordinates, occupancies and thermal parameters of $Ca_{0.6}Sr_{0.4}MoO_4$ composition are given in Table 1. The Rietveld discrepancy indices R_{wp}, R_p are around 8% and 5% respectively. Goodness of fit (χ^2) values are in the range of 1.2–2.0 which indicate that the patterns are well fitted with $I4_1/a$ space group and conforming the formation of tetragonal scheelite structure.

The unit cell representation of scheelite $Ca_{0.6}Sr_{0.4}MoO_4$ compound is shown in Fig. 3. The green, wine and blue colored spheres represent Mo, (Ca/Sr) and oxygen atoms respectively. It is seen from the Fig. 3 that the unit cell comprises of four formula units. This scheelite structure is composed with $(Ca/Sr)O_8$ bisdisphenoid and MoO_4 tetrahedra in which the $(Ca/Sr)O_8$ polyhedra arranged in zigzag manner along c-axis [30]. Each $(Ca/Sr)O_8$ polyhedra is surrounded by four $(Ca/Sr)O_8$ polyhedra and are connected by edge sharing. The MoO_4 tetrahedra are connected to the $(Ca/Sr)O_8$ polyhedra by sharing its corner with $(Ca/Sr)O_8$ polyhedra. The local environment of $(Ca/Sr)O_8$ bisdisphenoid and MoO_4 tetrahedra are shown in Fig. 4(a) and Fig. 4 (b) respectively.

In order to study the influence of Sr^{2+} substitution at A-site of $CaMoO_4$ compound on lattice vibrations of this compound, we have performed room temperature Raman spectroscopy measurements on $Ca_{1-x}Sr_xMoO_4$ (x= 0.0, 0.2, 0.4, 0.6, 0.8 and 1.0) compounds.

Fig. 5a shows the room temperature Raman spectra of $Ca_{1-x}Sr_xMoO_4$ (0, 0.2, 0.4, 0.6, 0.8, and 1.0) compositions in the frequency range 50–1000 cm^{-1}. It is clearly understood from these Raman spectra that, all these compositions form in scheelite structure with $I4_1/a$ space group [31]. The lattice vibrations in the scheelites structured compounds are categorized into internal modes which correspond to vibrations inside the $[MoO_4]^{2-}$ molecular units and external mode that are assigned to lattice vibrations of motion of M^{2+} metal ions and rigid $[MoO_4]^{2-}$ molecular units. The T_d symmetry of $[MoO_4]^{2-}$ tetrahedrons in free space is reduced to S_4 symmetry in crystal lattice due to crystal field effect. In scheelite structure the primitive cell possesses two $[MoO_4]^{2-}$ units consequently, the S_4 symmetry of $[MoO_4]^{2-}$ tetrahedron changes to C_{4h} that results to Davydov Splitting [13, 32]. As a result of crystal field effect and Davydov splitting, the degeneracy of $[MoO_4]^{2-}$ vibrations corresponding to T_d symmetry in free space is resolved. The group theoretical analysis predicts that 26 modes are possible in the case of tetragonal scheelite structured compounds with $I4_1/a$ space group which are distributed as irreducible representations.

$$\Gamma = 3A_g + 5B_g + 5E_g + 5A_u + 3B_u + 5E_u \quad (2)$$

Out of which the A_g, B_g and E_g vibrations are Raman active whereas A_u, B_u and E_u vibrations are IR active. In the present study 12 vibrational modes are observed for $Ca_{1-x}Sr_xMoO_4$ (0, 0.2, 0.4, 0.6, 0.8, and 1.0) compositions and are shown in **Fig. 5a**. In the Raman spectra, a dominant intense mode is observed at 881.7 cm^{-1} for x= 0.0 composition which is assigned to ν_s(Mo–O) (symmetric vibrations of Mo–O stretching mode, A_{1g}) and an antisymmetric stretching mode, ν_{as}(Mo–O) at 850.5 cm^{-1}. The modes below 350 cm^{-1} correspond to external modes, while internal modes are observed at higher wave number side. The assignment of all A_g, B_g and E_g modes are shown in Fig. 5a. With addition of higher ionic radius Sr^{2+} in the place of lower ionic Ca^{2+}, the unit cell volume increases which in turn affect the interatomic distances in the MoO_4 tetrahedra and causing the decrease in the covalence of

bond between cation and MoO_4. Out of these effects, the A_{1g} mode of $CaMoO_4$ shifts to lower wave number side with increase of Sr^{2+} substitution. However, we observed an anomaly in our present study. The increase in the internal symmetric stretching mode frequency (A_{1g}, Fig 5a) and decrease of maximum external mode frequency (E_g, Fig. 5b) result to the decrease of interaction between internal and external modes in $Ca_{1-x}Sr_xMoO_4$ (0, 0.2, 0.4, 0.6, 0.8, and 1.0) compounds. This combined affect shows impact on the shift and FWHM of A_{1g} mode in the case of end members (x=0.0 and 1.0). The A_{1g} mode becomes broader in the composition range $0.2 \leq x \leq 0.8$ that can be attributed to the presence of complex environment (presence of Ca^{2+} and Sr^{2+} ions in A-site) around the MoO_4 tetrahedron and influences the rigidity of tetrahedron in the scheelite structure.

3.2 Density and Microstructure

Densities of $Ca_{1-x}Sr_xMoO_4$ (x= 0.0, 0.2, 0.4, 0.6, 0.8 and 1.0) ceramic compositions were measured using Archimedes principle with an accuracy of ±0.005 whereas the theoretical densities of these ceramic compounds were calculated using the following equation [21].

$$\rho_{th} = \frac{nM}{NV}\ \text{g.cm}^{-3} \qquad (3)$$

Where n, M and V represent the number of formula units per unit cell, molecular weight and volume of these compounds whereas N represents the Avogadro's number (6.022×10^{23} mol^{-1}). All the measured (ρ_m) and theoretical densities (ρ_{th}) are given in Table. 2. From these we have calculated the percentage of theoretical density ($\rho = (\rho_m/\rho_{th})\times100$) of all these compounds and observed to possess more than 95% theoretical density. SEM micrographs of polished and thermally etched samples were collected by FEI quanta 400 high resolution Scanning Electron Microscope and are shown in Fig. 6(a)–(f). These micrographs reveal that all the samples are well densified and possess uniform grain size with less porosity. The densities of $Ca_{1-x}Sr_xMoO_4$ (x= 0.0, 0.2, 0.4, 0.6, 0.8 and 1.0) **ceramics** are given in Table 2.

3.3 Microwave Dielectric Properties

3.3.1 Dielectric constant (ε_r)

The dielectric constant of $Ca_{1-x}Sr_xMoO_4$ (x= 0.0, 0.2, 0.4, 0.6, 0.8 and 1.0) was measured by Hakki-Coleman method [28] at respective resonant frequency which vary in between 10 to 12 GHz. With increase in the Sr^{2+} the dielectric constant decreases from 9.6 to 7.4. According to Shannon additive rule with substitution of high polarizable Sr^{2+} (4.24 $Å^3$) ion in place of low polarizable Ca^{2+} (3.16 $Å^3$) ion [33], the dielectric constant should increase which is not observed in our present study. The dielectric constant mainly depends on the density, secondary phases [20, 34], ionic polarizability [25] and molar volume [35] of the compounds. From XRD patterns and microstructural analysis, it is observed that these compositions possess no secondary phases and possess more than 95% theoretical density. According to Clausius-Mosotti equation, dielectric constant depends on polarizability and molar volume of the compounds. In order to explain the contradiction in the dielectric constant variation and on which parameter it will depend, we calculated the rate of increase of molar volume (dV_m/dx) and ionic polarizability ($d\alpha_D/dx$) with Sr^{2+} substitution. It is noticed that the molar volume increases more rapidly than ionic polarizability and is shown in Fig. 7. Hence, molar volume plays predominant role in the variation of dielectric constant of $Ca_{1-x}Sr_xMoO_4$ (x= 0.0, 0.2, 0.4, 0.6, 0.8 and 1.0) system.

As the dielectric constant depends on the density and porosity of the samples, the measured values of dielectric constant are corrected to the porosity using the following formula [17].

$$\varepsilon_r = \varepsilon_{\text{exp.}}(1+1.5P) \quad (4)$$

where ε_r, ε_{exp} are the porosity corrected and experimentally observed dielectric constants

and $P = 1 - \frac{\rho_m}{\rho_{\text{th.}}}$

ρ_m: measured density, ρ_{th}: Theoretical density.

The porosity corrected dielectric constants of these compositions are given in Table 2. The variation in ε_r of $Ca_{1-x}Sr_xMoO_4$ (x= 0.0, 0.2, 0.4, 0.6, 0.8 and 1.0) compositions is correlated with the molar volume (V_m) of these compositions and is shown in Fig. 8.

3.3.2 Quality factor

Quality factor ($Q \times f$) of all the $Ca_{1-x}Sr_xMoO_4$ (0, 0.2, 0.4, 0.6, 0.8 and 1.0) ceramics were measured using reflection cavity technique with gold coated copper cavity at the respective resonant frequencies which are in the frequency range 10 to 12 GHz and are shown in Fig. 9. The quality factor decreases from 51500 GHz at x = 0.0 to a minimum value 35500 GHz at x=0.4 compound and again increased to 48500 GHz at x=1.0. It is well known that the quality factor of microwave dielectric ceramics depends on extrinsic losses which arises from the presence of defects, secondary phases, grain size and porosity where as the intrinsic losses are related to crystal structure and bonding character of ions of the materials [36-40]. The effect of extrinsic losses are minimal as the Rietveld refinement reveals that there are no secondary phases present in $Ca_{1-x}Sr_xMoO_4$ (0, 0.2, 0.4, 0.6, 0.8 and 1.0) and microstructural analysis indicate that all the compounds possess uniform grain size with less porosity.

Quality factor predominantly depends on the bond parameters such as bond strength [41, 42]. Weakly bounded cations with oxygen will give additional dielectric loss, because the ions rattle more freely in the MoO_4 tetrahedron and interact strongly with the anharmonic phonons. The Mo-O bond strength in $Ca_{1-x}Sr_xMoO_4$ (0, 0.2, 0.4, 0.6, 0.8, and 1.0) compounds were calculated using the following equations

$$V_i = \sum_j v_{ij} \tag{5}$$

$$v_{ij} = \exp\left\{\frac{R_{ij} - d_{ij}}{b}\right\} \tag{6}$$

where R_{ij} is the bond valence parameter, d_{ij} is the bond length between i and j atoms and b is commonly taken as universal constant equal to 0.37 Å. The Mo-O bond lengths are

obtained by Rietveld refinement. The obtained bond valence sum is used to calculate the bond strength (*S*) which is defined as the ratio of bond valence sum of cation and its coordination number. The variation of Mo-O bond strength in all these $Ca_{1-x}Sr_xMoO_4$ (0, 0.2, 0.4, 0.6, 0.8, and 1.0) compositions is shown in Fig. 9. It can be observed that the variations in both quality factor and Mo-O bond strength with Sr substitution are analogous to each other and are given in Table 3.

3.3.3 Temperature coefficient of resonant frequency (τ_f)

The temperature coefficient of resonant frequency (τ_f) is related to temperature coefficient of dielectric constant (τ_ε) as

$$\tau_f = -\alpha_1 - \frac{1}{2}\tau_\varepsilon \tag{7}$$

In the above equation 'α_1' is the coefficient of thermal expansion and is in the range of 10 ppm/^{o}C for all the ceramics. So τ_f mainly depends on temperature coefficient of dielectric constant (τ_ε). Form Clausius-Mosotti equation, τ_ε can be derived from following expression.

$$\tau_\varepsilon = \frac{1}{\varepsilon}\left(\frac{\partial \varepsilon}{\partial T}\right) = \frac{(\varepsilon - 1)(\varepsilon + 2)}{\varepsilon}(A + B + C) \tag{8}$$

Where $A = -\frac{1}{3V}\left(\frac{\partial V}{\partial T}\right)_P \qquad B = \frac{1}{3\alpha_m}\left(\frac{\partial \alpha_m}{\partial V}\right)_T \left(\frac{\partial V}{\partial T}\right)_P \qquad C = \frac{1}{3\alpha_m}\left(\frac{\partial \alpha_m}{\partial T}\right)_V$

Where 'α_m' and 'V' represents the polarizability and volume of macroscopic, small sphere respectively.

The term *A* gives the dependence of polarizability on the temperature and is always negative because of anharmonic effect of potential well where the ions will vibrate. With increase in temperature, the polarizability of constant number of dipoles will increase because of volume expansion and is given by term *B*. According to Bosman and Havinga [43], the first two terms *A* and *B* are related with the volume expansion which are nearly of equal magnitude but opposite in sign, therefore the effect of *A* and *B* on τ_ε is negligible. The third term *C* gives the restoring force acting on the ions and this restoring force depends on the shape of the

potential well, hence the term *C* is explained with the structural parameters of the constituent elements in the compounds.

In general, temperature coefficient of capacitance (TCC) is directly proportional to temperature of coefficient of dielectric constant (τ_ε) [44]. Diao *et al.* observed that the temperature coefficient of capacitance (TCC) decreases with increase Raman shift [35]. From this, it is clearly understood that the τ_f depends on Raman shift. In our present work, from Raman spectra (fig. 5a), it is clearly seen that with Sr^{2+} substitution A_{1g} mode is shifting towards the higher wavenumber side (from 881.7 cm^{-1} of x = 0.0 compound to 889.8 cm^{-1} of x = 1.0) whereas highest external mode E_g (fig. 5b) is moving towards the lower wavenumber side (from 270.6 cm^{-1} for x = 0.0 compound to 235.4 cm^{-1} for x = 1.0) which inturn influences the rigidity of cation and oxygen environment and decrease the restoring force required to recover the degree of distortion of oxygen polyhedra. The temperature coefficient of resonant frequency of ABO_4 ceramic compounds is observed to be influenced by the complex environment around the oxygen polyhedra [20]. In $Ca_{1-x}Sr_xMoO_4$ (x=0.0, 0.2, 0.4, 0.6, 0.8 and 1.0) compositions, with increase in Sr^{2+} content the τ_f values varied from -28 to -17 ppm/^oC. This variation in τ_f could be attributed to bonding characteristics of cation oxygen polyhedra which influences the Raman shift of A_{1g} mode. The Raman shift and τ_f values are given in Table 3 and the variation both these parameters with Sr^{2+} substitution is shown in Fig. 10.

3.4 Optical Properties

The optical properties of $Ca_{1-x}Sr_xMoO_4$ (x=0.0, 0.2, 0.4, 0.6, 0.8 and 1.0) compositions were studied by collecting the optical absorption (OA) of these compositions. The optical absorption spectra of these compositions in 340–550 nm range are shown in Fig. 11 and is observed that the absorption edge shifts from 394 nm for x = 0.0 to 369 nm for x = 1.0. The relation between optical band gap, absorbance and photon energy is given as [45].

$$h\upsilon\alpha \propto \left(h\upsilon - E_g^{opt}\right)^{n/2} \quad (9)$$

Where 'α' is the absorbance, 'h' is plank's constant, 'υ' is the frequency and 'E_g^{opt}' is optical bang gap. The value of 'n' depends on the characteristics of transition in a material *i.e.* n = 1 for direct band gap materials and n = 4 for indirect bang gap material. The bang gap of $Ca_{1-x}Sr_xMoO_4$ (x=0.0, 0.2, 0.4, 0.6, 0.8 and 1.0) compositions were estimated by extrapolating the linear region on the higher photon energy region of $(\alpha h\upsilon)^2$ versus photon energy ($h\upsilon$) plots that are not shown here. The observed band gap of $CaMoO_4$ and $SrMoO_4$ samples are 3.30 eV and 3.51 eV and slightly deviated from the reported values which may be attributed to the large grain size and intrinsic defects in the samples [31, 46]. With Sr^{2+} substitution the band gap increases from 3.30 eV to 3.51 eV. We also observed a non linear variation in the band gap with Sr^{2+} substitution and is shown in Fig. 12. Osamura *et al.* explained the non linear behavior of band gap in $Ga_{1-x}In_xN$ thin films with help of Bowing effect [47]. So in order to explain the non linear behavior in band gap of $Ca_{1-x}Sr_xMoO_4$ (x=0.0, 0.2, 0.4, 0.6, 0.8 and 1.0) compounds with help of Bowing effect, the observed band gap values were fitted with the following equation yielding a smaller 'c' value 0.17 eV [48].

$$E_g = (1-x)E_{g,A} + xE_{g,B} + cx(1-x) \quad (10)$$

where $E_{g,A}$, $E_{g,B}$ are band gap of $CaMoO_4$ and $SrMoO_4$ respectively. 'c' is the Bowing parameter which is effected by atomic size difference and chemical ionicity mismatch and 'x' is the concentration of Sr^{2+}. It is clear from the Fig. 12 that, the observed values are well fitted with the Bowing equation.

Conclusions

The $Ca_{1-x}Sr_xMoO_4$ (x = 0.0, 0.2, 0.4, 0.6, 0.8 and 1.0) ceramic compositions were successfully prepared via conventional solid state reaction method and all the compositions were observed to possesses tetragonal scheelite structure with $I4_1/a$ space group. All these

compounds possess more than 95% theoretical density. The effect of Sr^{2+} substitution on the bonding characteristics and microwave dielectric properties was studied with help of Rietveld refinement and Raman spectra of these compositions. The microwave dielectric properties such as dielectric constant (ε_r) and quality factor ($Q\times f$) were correlated with the molar volume (V_m) and Mo-O bond strength of these compositions respectively. Temperature coefficient of resonant frequency (τ_f) was explained with Raman shift of A_{1g} mode in these compositions. Well dense samples possess good microwave dielectric properties (ε_r= 6.5 – 9.7, $Q\times f$ = 35000 –52000 GHz, τ_f = -28 to -17 ppm/^{o}C). The non linear variation in the band gap of these compositions and was fitted the bowing equation.

Acknowledgements

The authors are thankful to University Grant Commission, New Delhi, India for providing financial assessment in the form of Senior Research Fellowship.

References

[1] I.M. Reaney, D. Iddles, J. Am. Ceram. Soc. 89 (2006) 2063–2072.

[2] R.J. Cava, J. Mater. Chem. 11 (2001) 54–62.

[3] C.F. Tseng, C.L. Huang, N.R. Yang, C.H. Hsu, J. Am. Ceram. Soc. 89 (2006) 1465–1470.

[4] H. Matsumoto, H. Tamura, K. Wakino, Jpn. J. Appl. Phys. 30 (1991) 2347–2349.

[5] S. Kawashima, M. Nishida, I. Ueda, H. Ouchi, J. Am. Ceram. Soc. 66 (1983) 421–423.

[6] M. Daturi, G. Busca, M.M. Borel, A. Leclaire, P. Piaggio, J. Phys. Chem. B. 101 (1997) 4358–4369.

[7] G.K. Choi, J.R. Kim, S.H. Yoon , K.S. Hong, J. Eur. Ceram. Soc. 27 (2007) 3063–3067.

[8] L. Hoffart, U. Heider, L. Jorissen, R.A. Huggins, W. Witschel, Ionics. 1 (1995) 131–135.

[9] B. Yan, J.H. Wu, Mater. Chem. Phys. 116 (2009) 67–71.

[10] I.A. Kamenskikha, V.N. Kolobanova, V.V. Mikhailina, L.I. Potkinc, I.N. Shpinkova, D.A. Spasskya, B.I. Zadneprovskyc, G. Zimmerer, Nucl. Instrum. Methods. Phys. Res. Sect. A 470 (2001) 270–273.

[11] M. Itoh, M. Fujita, Phy. Rev. B 62 (2000) 12825–12830.

[12] A.S. Barker, Jr, Phy. Rev. 135 (1964) A742–A747.

[13] S.P.S. Porto, J.F. Scott, Phy. Rev. 157 (1967) 716–719.

[14] K. Hara, H. Takenaka, Y. Ishibashi, J. Phy. Soc. Japan. 57 (1988) 3220–3225.

[15] D. Zhou, L- X. Pang, J. Guo, Z.-M. Qi, T. Shao, X. Yao, C. A. Randall, J**. Mater. Chem.** 22 **(**2012) 21412-21419.

[16] D. Zhou, J. Guo, X. Yao, L.-X. Pang, Z.-M. Qi, T. Shao, Funct. Mater. Lett. 5 (2012) 1250042-1250047.

[17] S.H. Yoon, D.W. Kim, S.Y. Cho, K.S. Hong, J. Eur. Ceram. Soc. 26 (2006) 2051–2054.

[18] R.C. Pullar, S. Farrah, N.M. Alford, J. Eur. Ceram. Soc. 27 (2007) 1059–1063.

[19] E.S. Kim, S.H. Kim, J. Electroceram. 17 (2006) 471–477.

[20] E.S. Kim, B.S. Chun, R. Freer, R.J. Cernik, J. Eur. Ceram. Soc. 30 (2010) 1731–1736.

[21] Q. Liao, L. Li, X. Ren, X. Ding, J. Am. Ceram. Soc. 94 (2011) 3237-3240.

[22] E.S. Kim, C.J. Jeon, P.G. Clem, J. Am. Ceram. Soc. 95 (2012) 2934–2938.

[23] D. Zhou, C.A. Randall, L.X. Pang, H. Wang, J. Guo, G.Q. Zhang, Y. Wu, K.T. Guo, L. Shui, X. Yao, Mater. Chem. Phys. 129 (2011) 688–692.

[24] D. Zhou, C.A. Randall, H. Wang, L.X. Pang, X. Yao, J. Am. Ceram. Soc. 93 (2010) 2147–2150.

[25] S.D.R. Rao, S. Roopas Kiran ,V.R.K. Murthy, J. Am. Ceram. Soc. 95 (2012) 3532–3537.

[26] A.C. Larson, R.B. von Dreele, General Structural Analysis System (GSAS), Los Alamos National Laboratories, Los Alamos, NM, 1990.

[27] B.H. Toby, J. Appl. Crystallogr. 34 (2001) 210–213.

[28] B.W. Hakki, P.D. Coleman, IRE Trans. Microwave. Theory. Tech. 8 (1960) 402–410.

[29] R.D. Shannon, Acta. Cryst. A 32 (1976) 751–767.

[30] S.N. Achary, S.J. Patwe, P.S.R. Krishna, A.B. Sindhe, A.K. Tyagi, J. Alloy. Compd. 438 (2007) 274–278.

[31] J.C. Sczancoski, L.S. Cavalcante, M.R. Joya, J.A. Varela, P.S. Pizani, E. Longo, Chem. Eng. J. 140 (2008) 632 –637.

[32] W. Cockbain, The Dynamics of Atoms in Crystals. Edward Arnold: London; 1973.

[33] R.D. Shannon, J. Appl. Phys. 73 (1993) 348–366.

[34] S.J. Penn, N.M. Alford, A. Templeton, X. Wang, M. Xu, M. Reece, K. Scherapel, J. Am. Ceram. Soc. 80 (1997) 1885–1888.

[35] C. Diao, F. ShiF, J. Phys. Chem. C 116 (2012) 6852–6858.

[36] M.H. Liang, C.T. Hu, H.F. Cheng, I.N. Lin, J. Steeds, J. Eur. Ceram. Soc. 21 (2001) 2759–2763.

[37] W.S. Kim, E.S. Kim, K.H. Yoon, J. Am. Ceram. Soc. 82 (1999) 2111–2116.

[38] S. Roopas Kiran, G. Sreenivasulu, V.R.K. Murthy, V. Subramanian, B.S. Murthy, J. Am. Ceram. Soc. 95 (2012) 1973–1979.

[39] X.C. Fan, X.M. Chen, X.Q. Liu, Chem. Mater. 20 (2008) 4092–4098.

[40] A. Dias, G. Subodh, M.T. Sebastian, M.M. Lage, R.L. Moreira, Chem. Mater. 20 (2008) 4347–4355.

[41] L.S. Cho, J.S. Lee, S.T. Bae, J.R. Kim, K.S. Hong, J. Electroceram. 23 (2009) 154–158.

[42] M.W. Lufaso, Chem. Mater. 16 (2004) 2148–2156.

[43] A.J. Bosman, E.E. Havinga, Phys. Rev 129 (1963) 1593–1600.

[44] A.M. Azad, T.Y. Pang, M.A. Alim, Active. and Passive. Elec. Comp. 26 (2003)151–166

[45] D.L. Wood, J. Tauc, Phys. Rev. B 5 (1972) 3144–3151.

[46] Y. Zhang, N.A.W. Holzwarth, R.T. Williams, Phys. Rev. B 57 (1998) 12738–12750.

[47] K. Osamura, S. Naka, Y. Murakami, J. Apl. Phy. 46 (1975) 3432–3437.

[48] H.L. Shi, Y. Duan, Eur. Phys. J. B 66 (2008) 439–444.

Fig. 1. Room temperature XRD patterns of $Ca_{1-x}Sr_xMoO_4$ compounds.

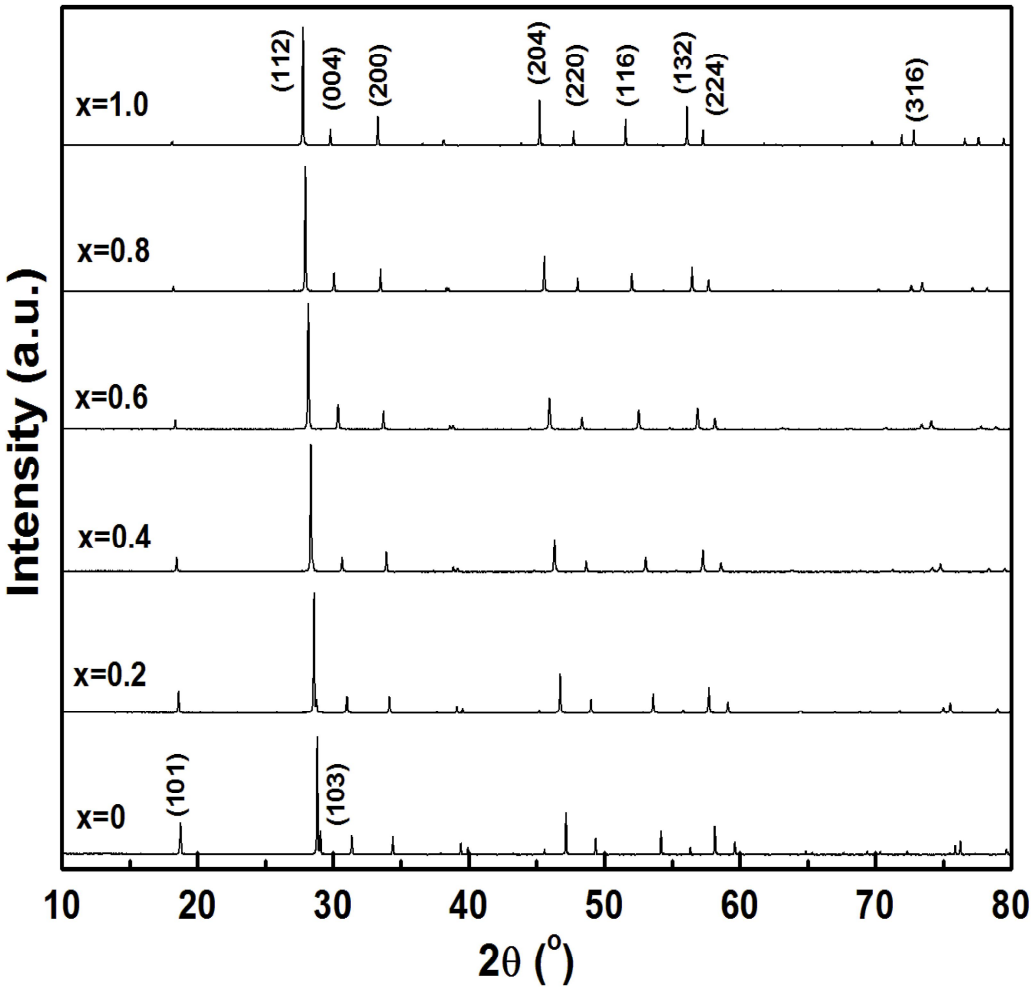

Fig. 2. Rietveld refinement plot of $Ca_{0.6}Sr_{0.4}MoO_4$ compound.

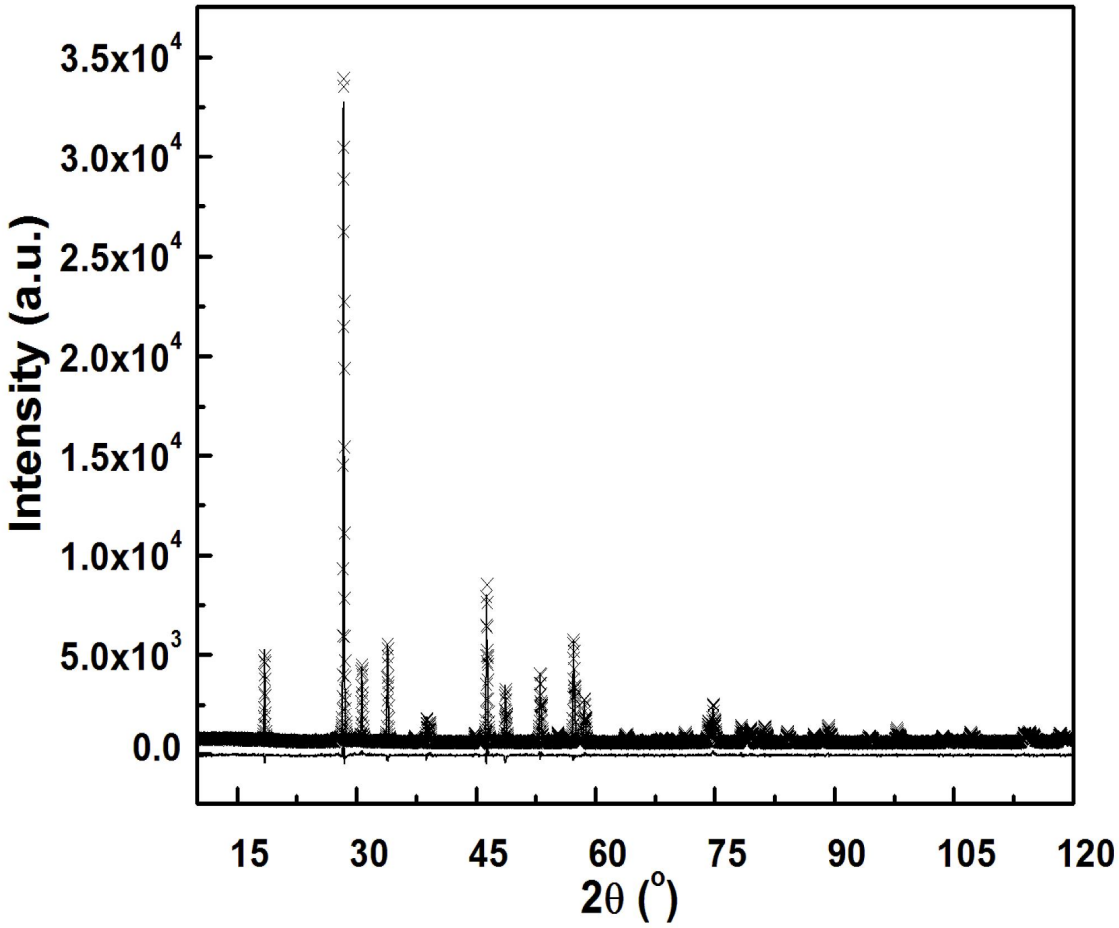

Fig. 3. Unit cell representation of $Ca_{0.6}Sr_{0.4}MoO_4$ (along b-axis view).

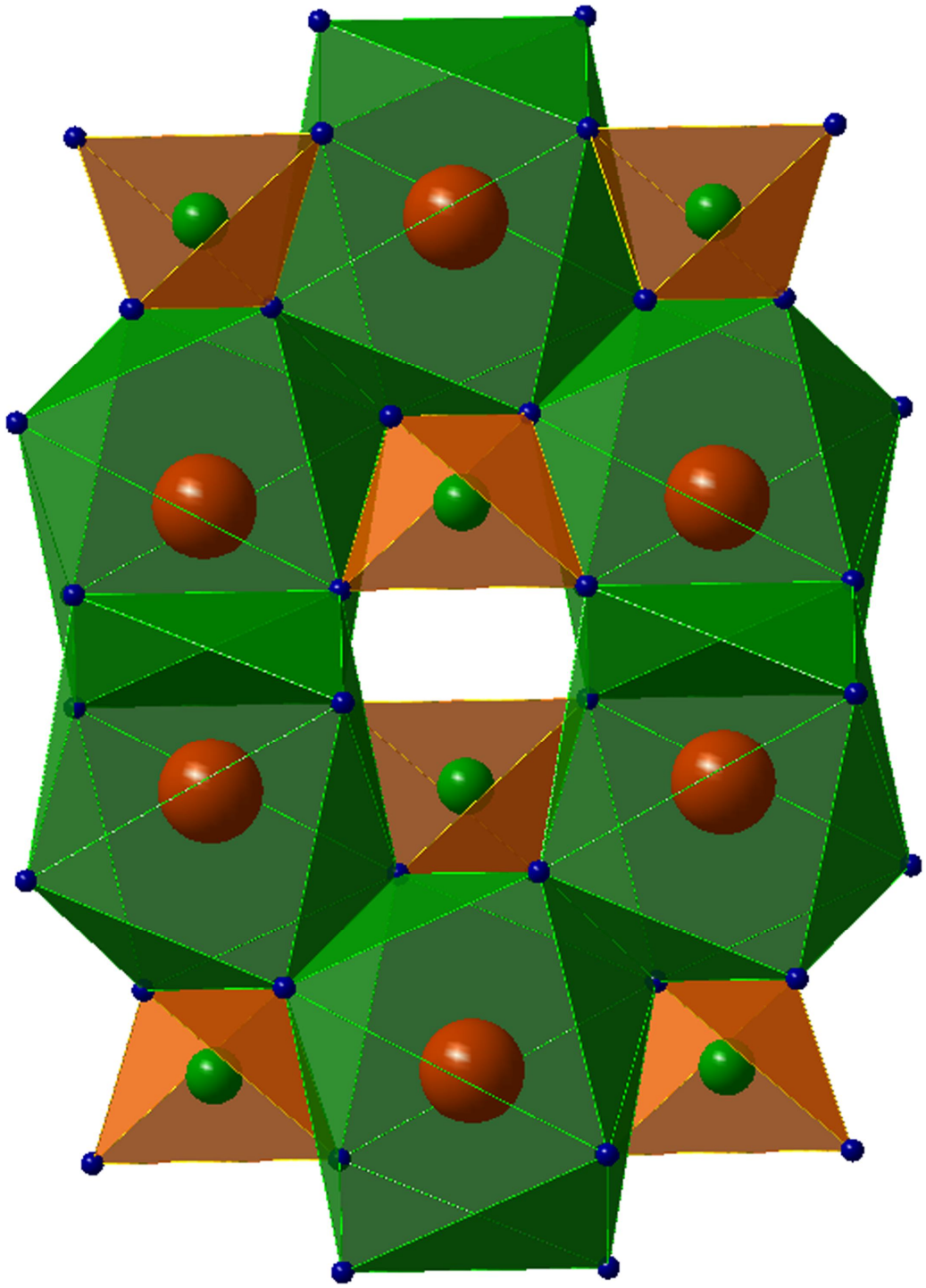

Fig. 4a. Local environment of $(Ca/Sr)O_8$ bisdisphenoid (c-axis view) in scheelite structure.

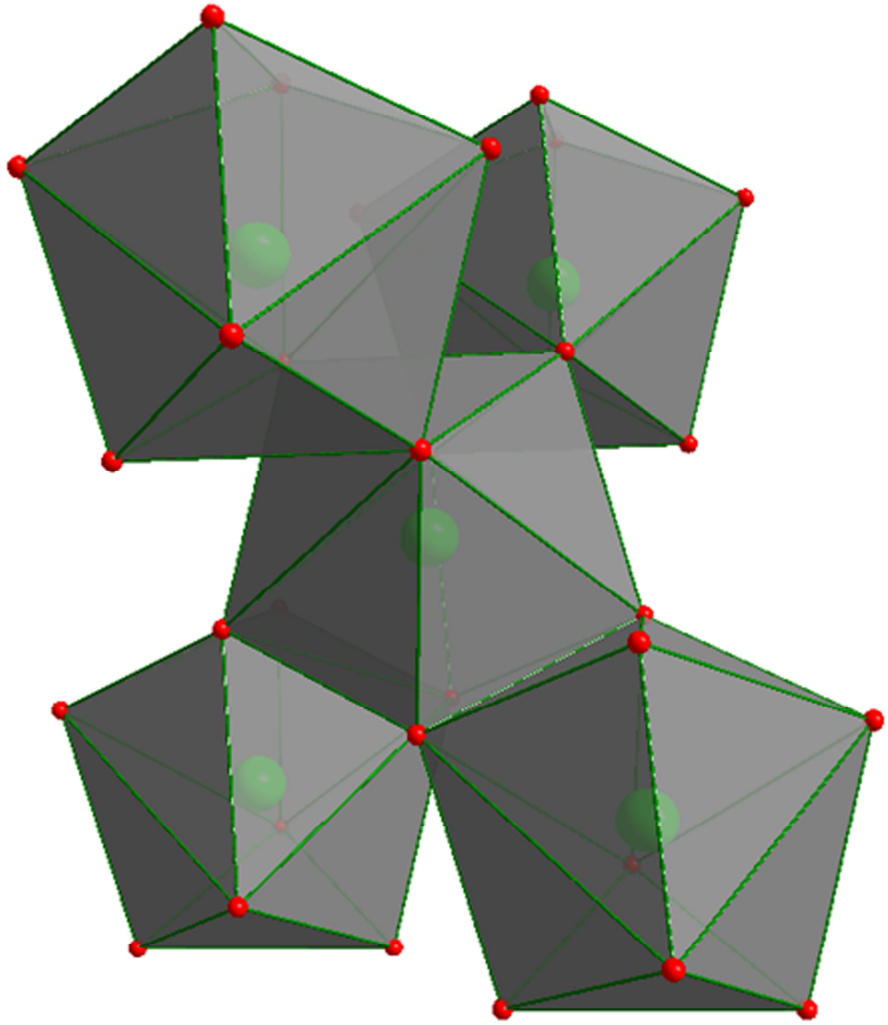

Fig. 4b. Local environment of MoO_4 (along c-axis view) tetrahedra in scheelite structure.

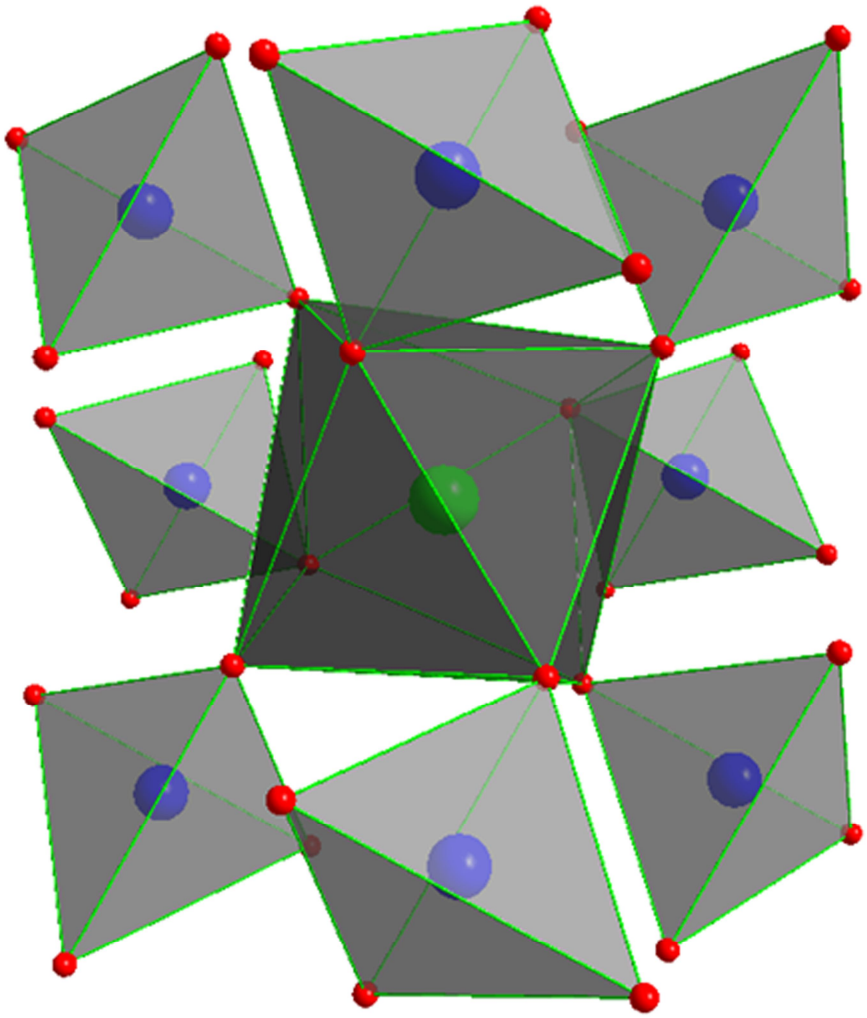

Fig. 5a. Room temperature Raman spectra of $Ca_{1-x}Sr_xMoO_4$ compounds.

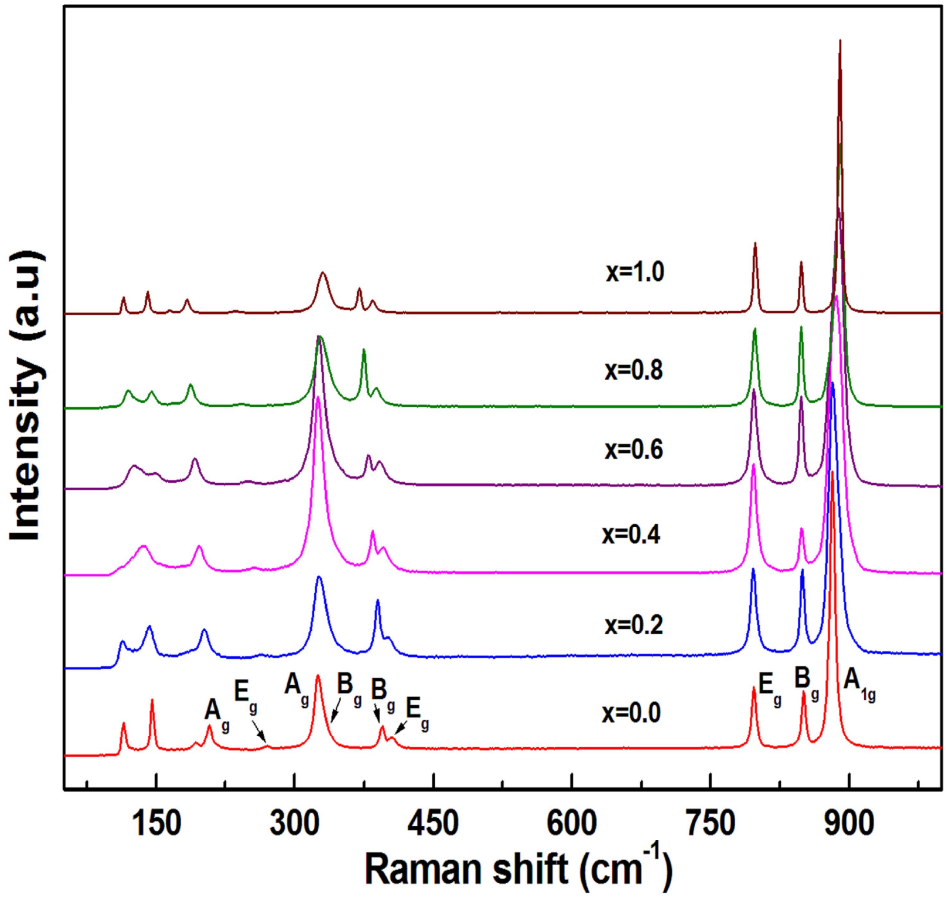

Fig. 5b. Raman spectra of $Ca_{1-x}Sr_xMoO_4$ compounds (150–350 cm^{-1}).

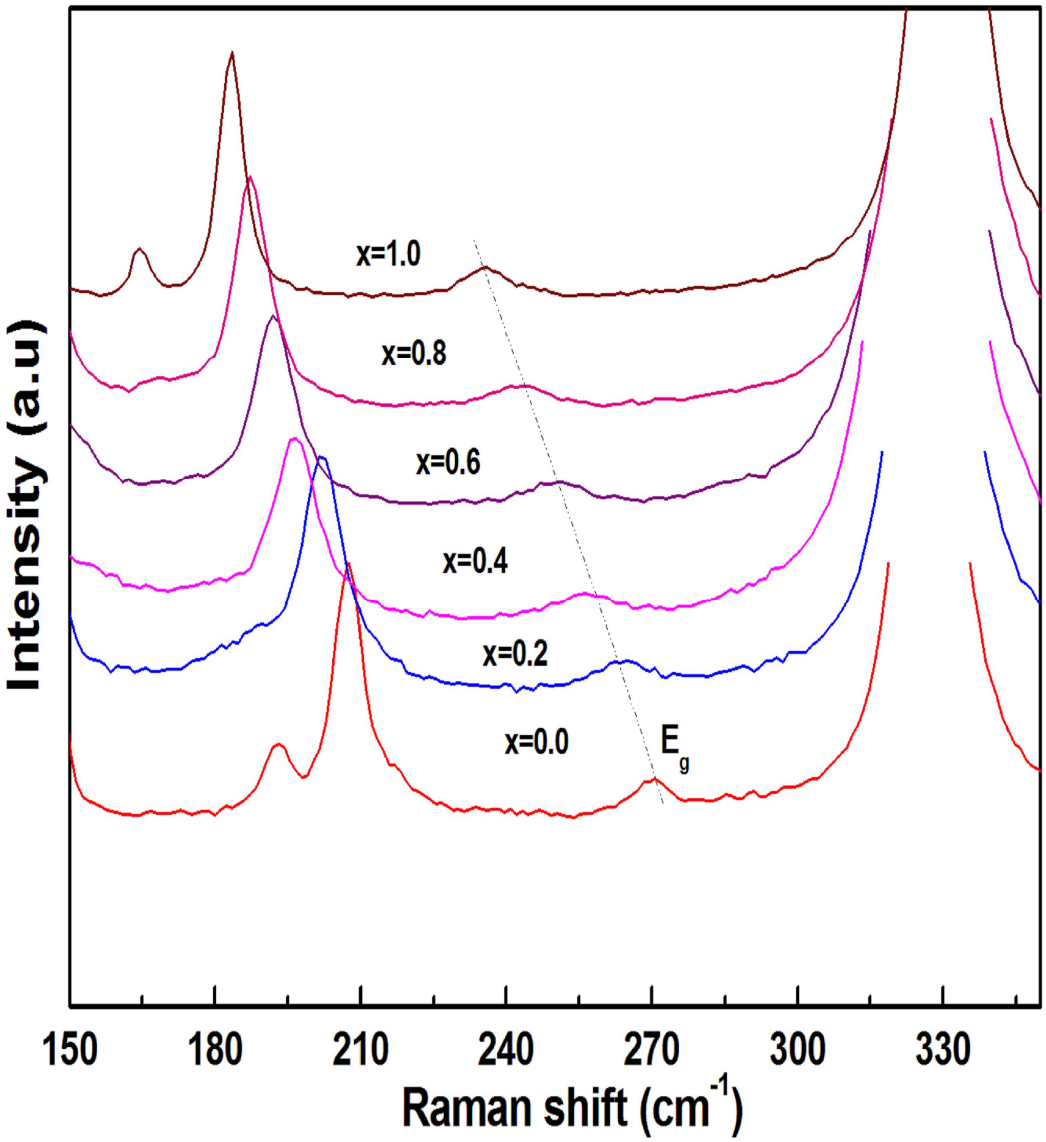

Fig. 6(a-f). SEM micrographs of $Ca_{1-x}Sr_xMoO_4$ compounds.

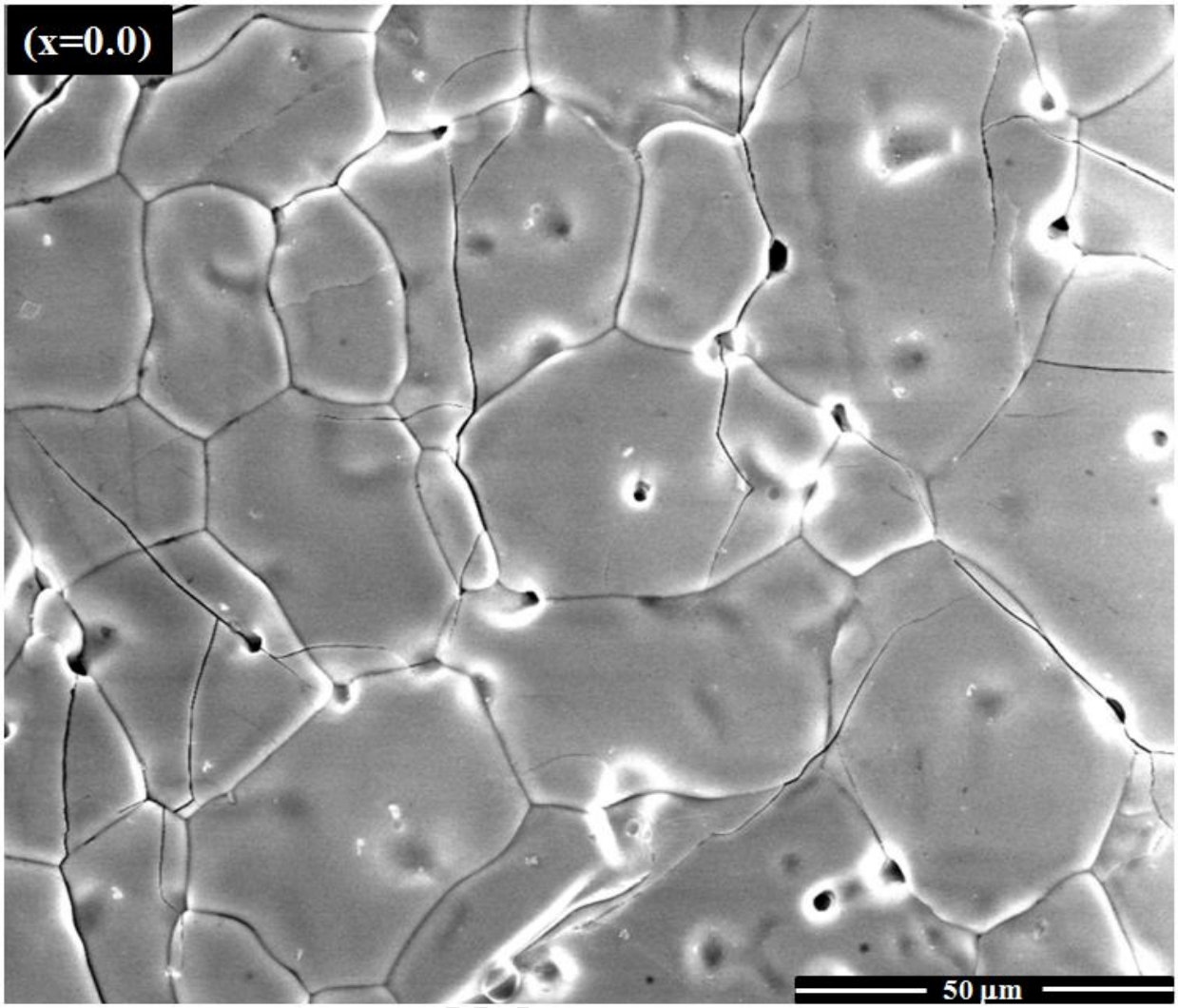

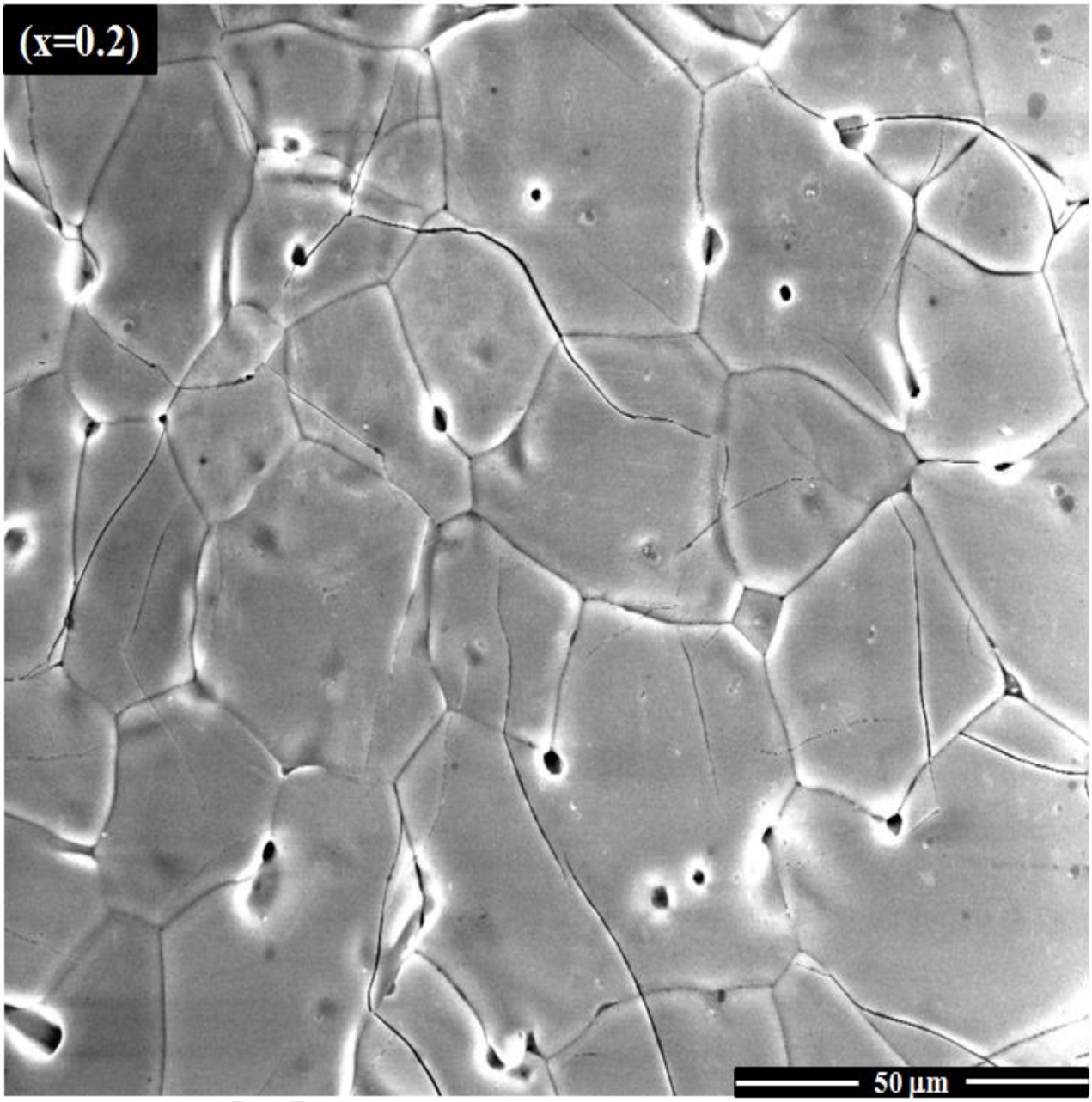

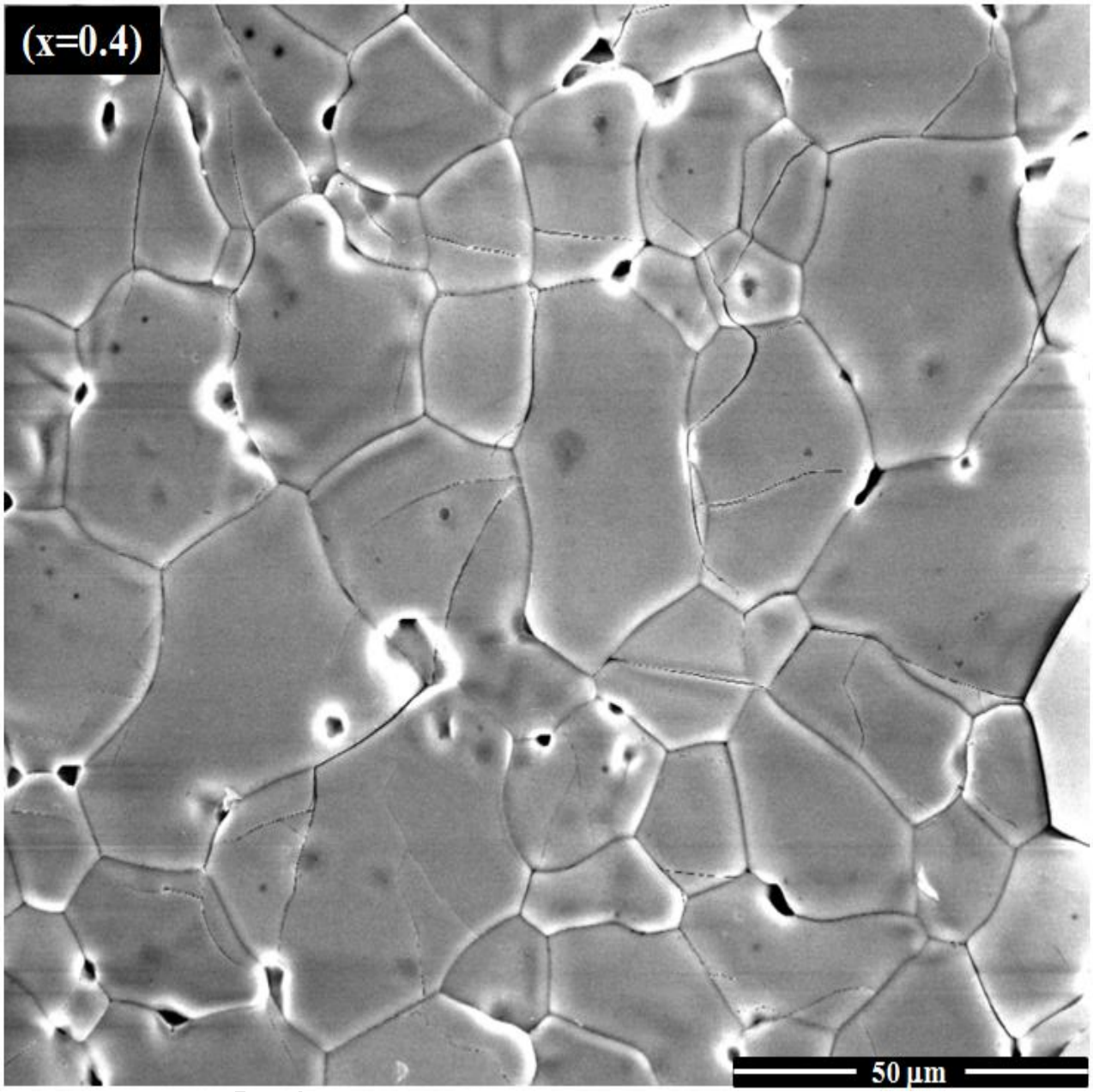

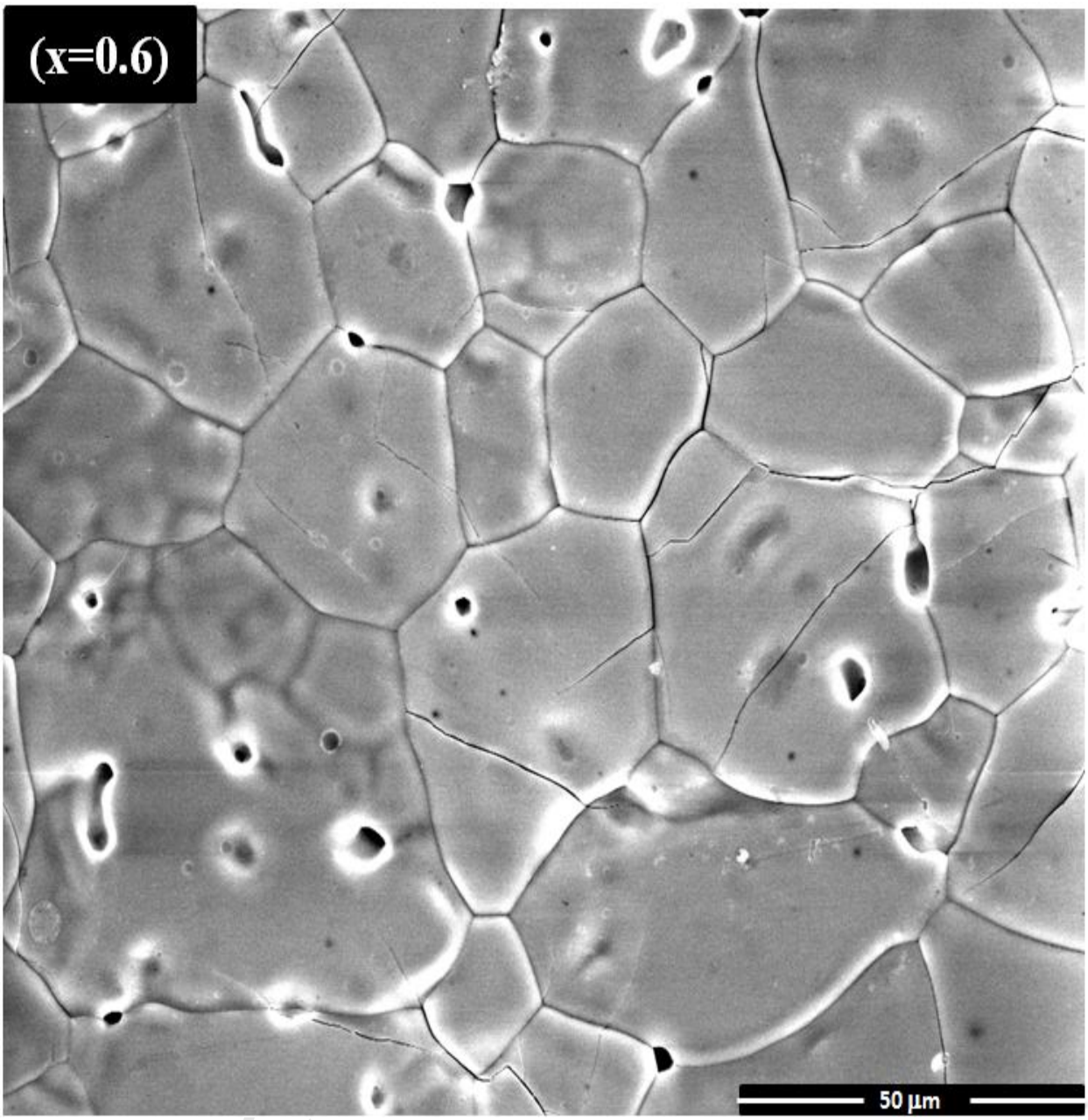

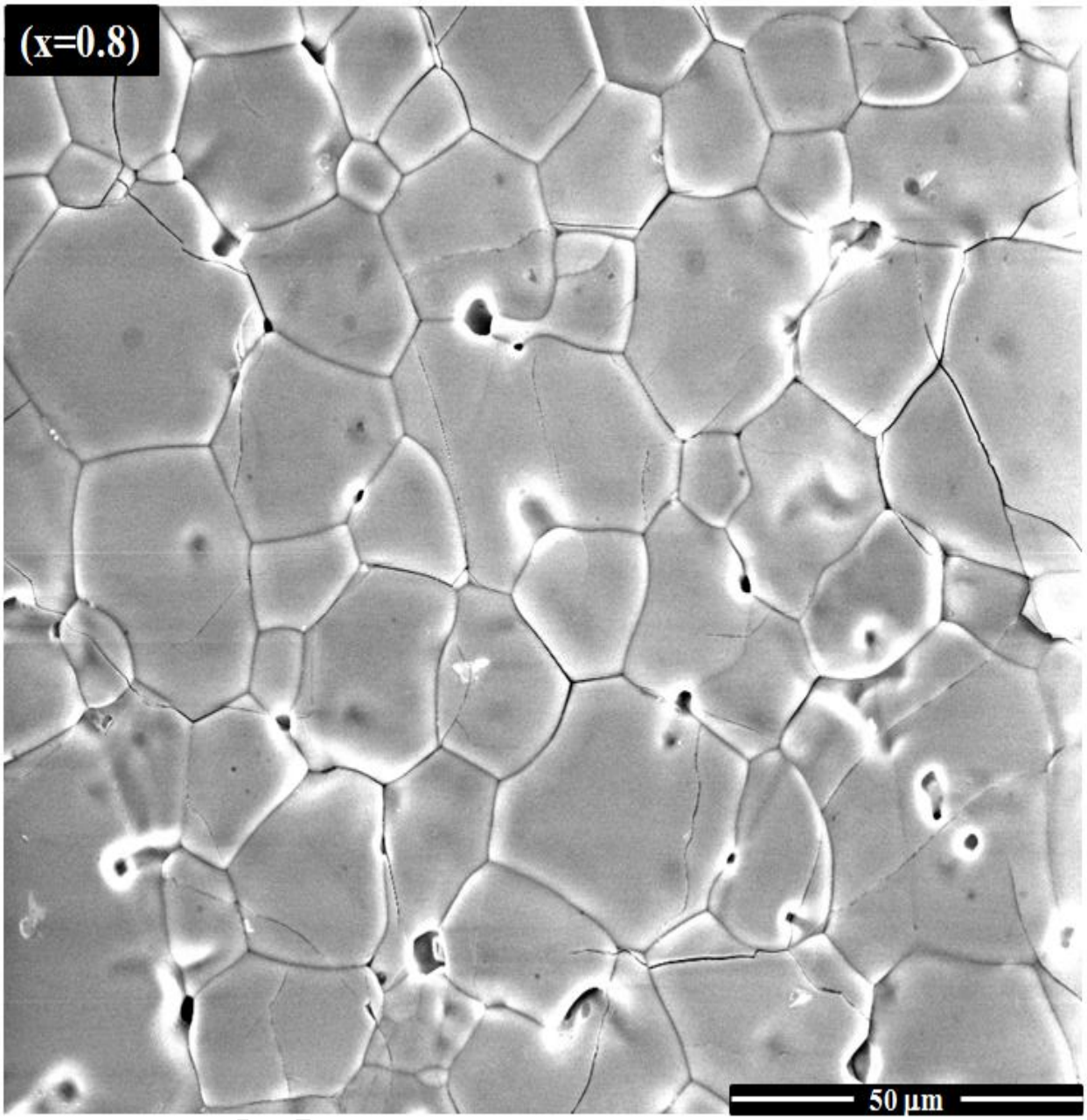

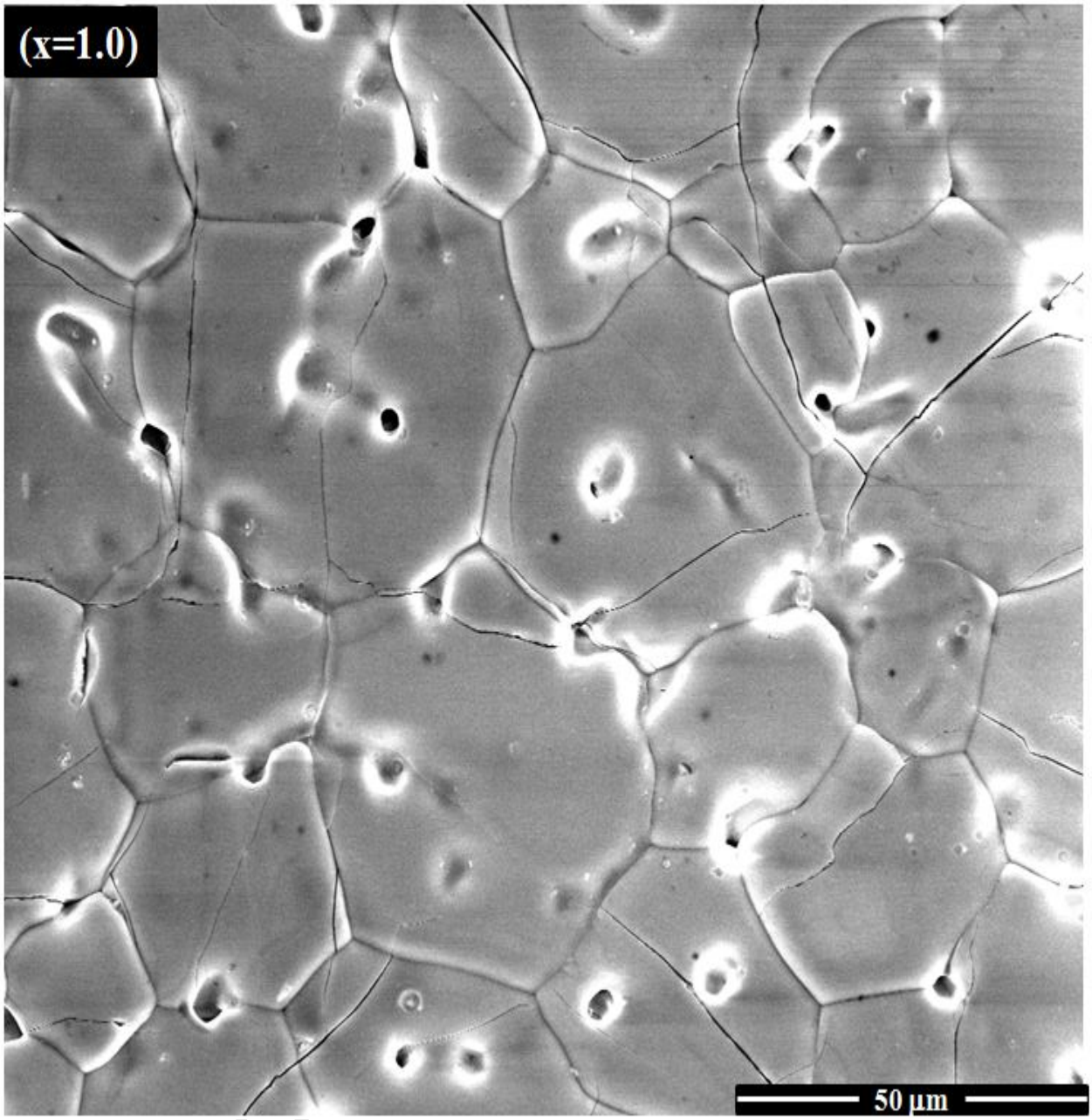

Fig. 7. Rate of change of molar volume and ionic polarizability of $Ca_{1-x}Sr_xMoO_4$ compounds.

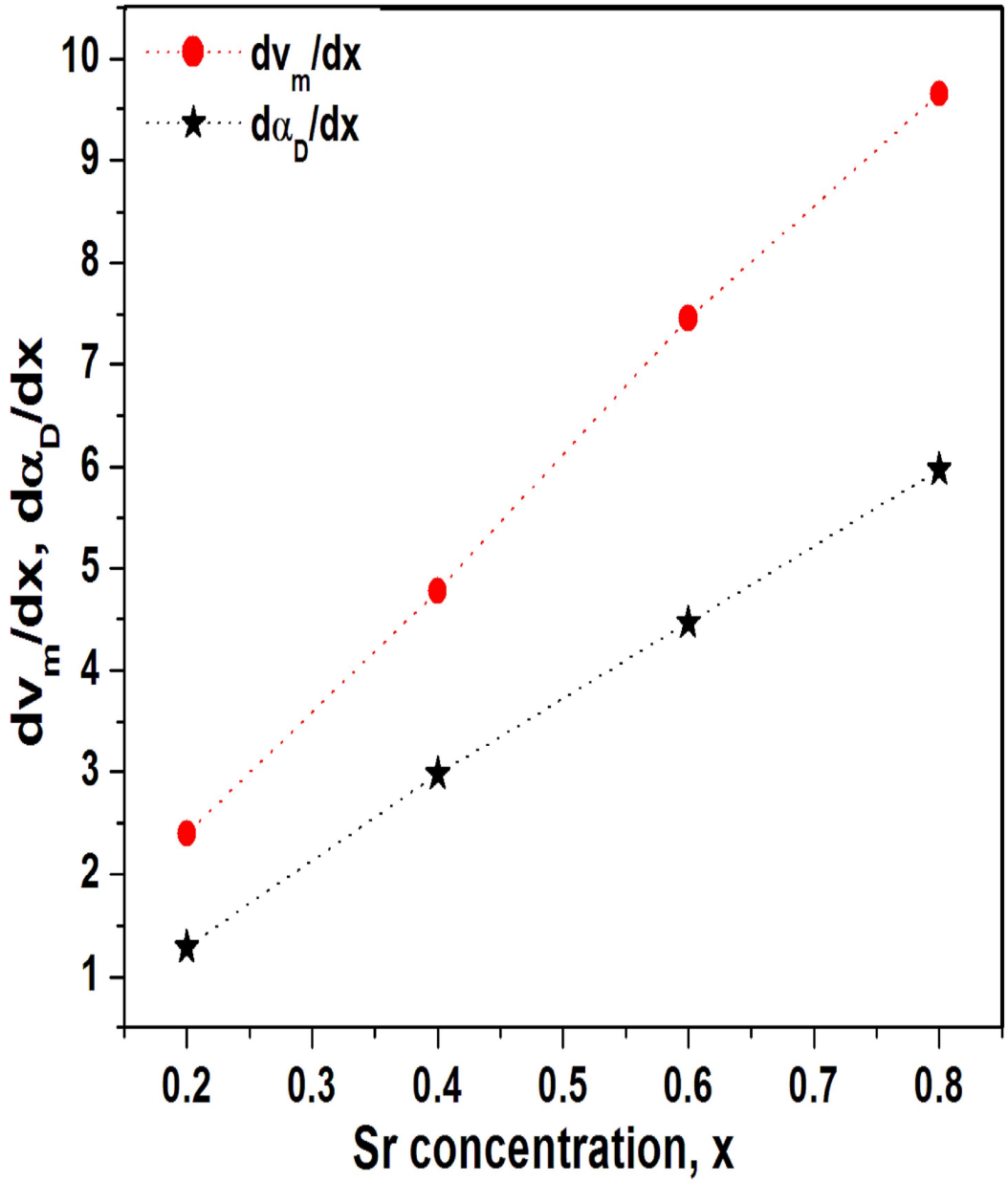

Fig. 8. Variation of dielectric constant with molar volume of $Ca_{1-x}Sr_xMoO_4$ compounds.

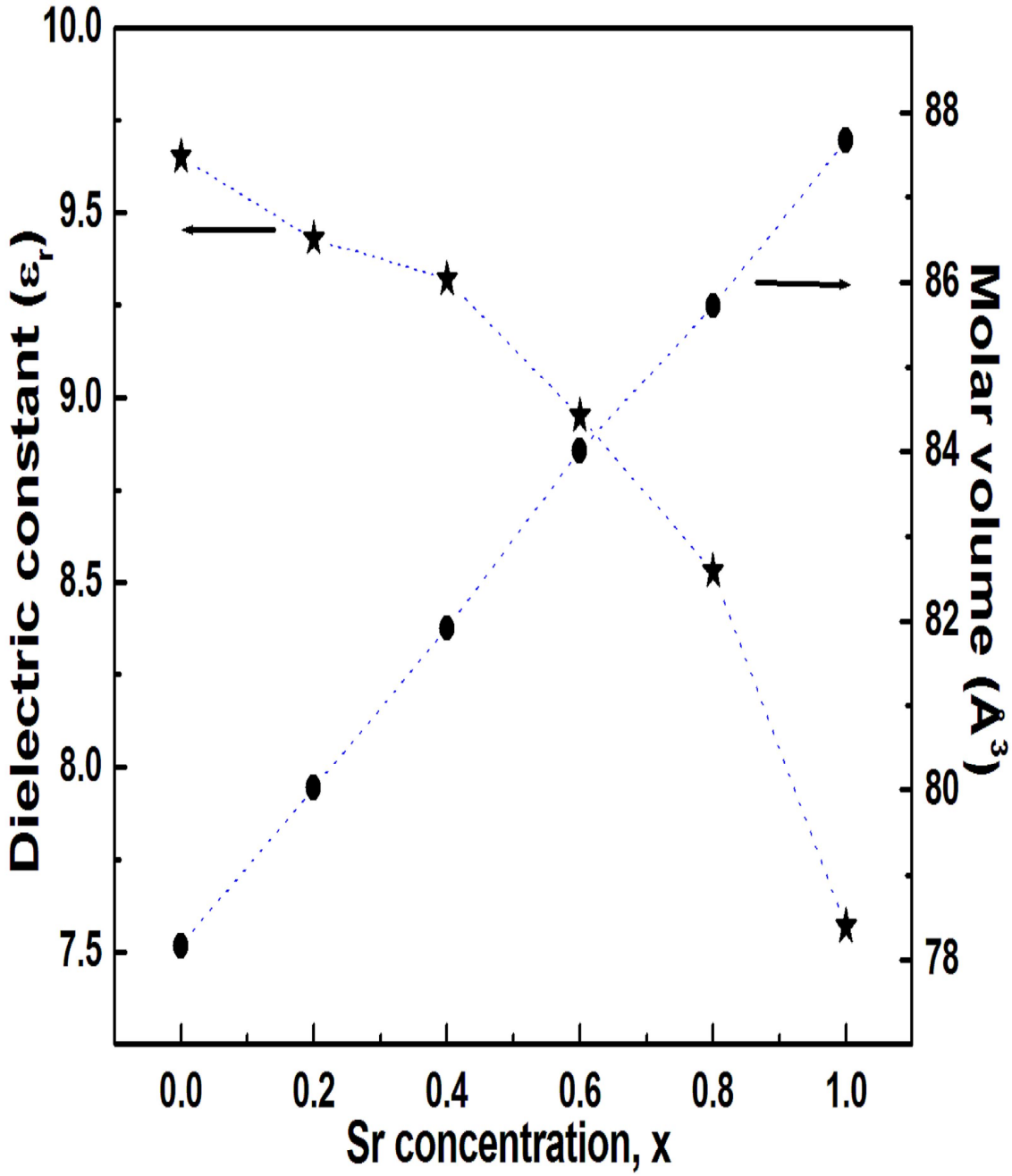

Fig. 9. Variation of quality factor and Mo-O bond strength in $Ca_{1-x}Sr_xMoO_4$ compounds.

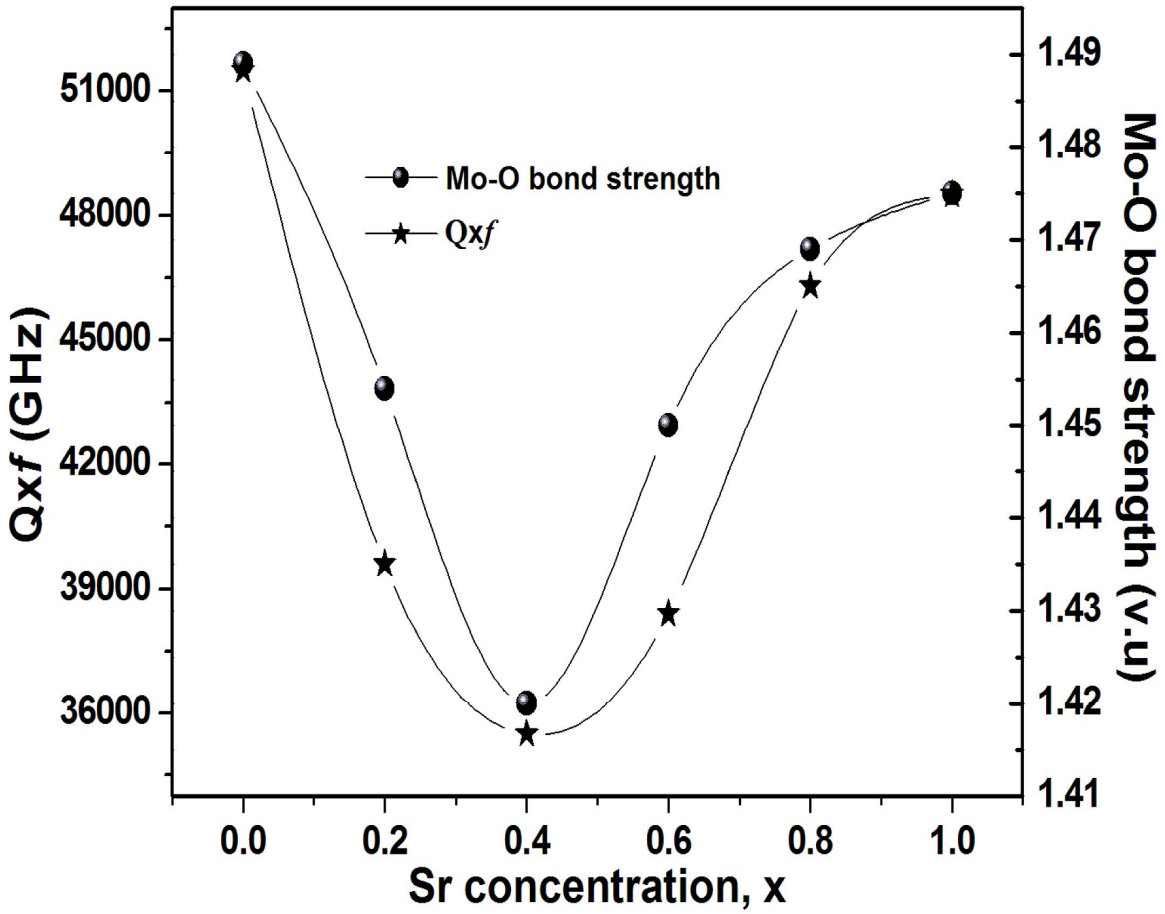

Fig. 10. Variation of τ_f and Raman shift of A_{1g} mode of $Ca_{1-x}Sr_xMoO_4$ compounds.

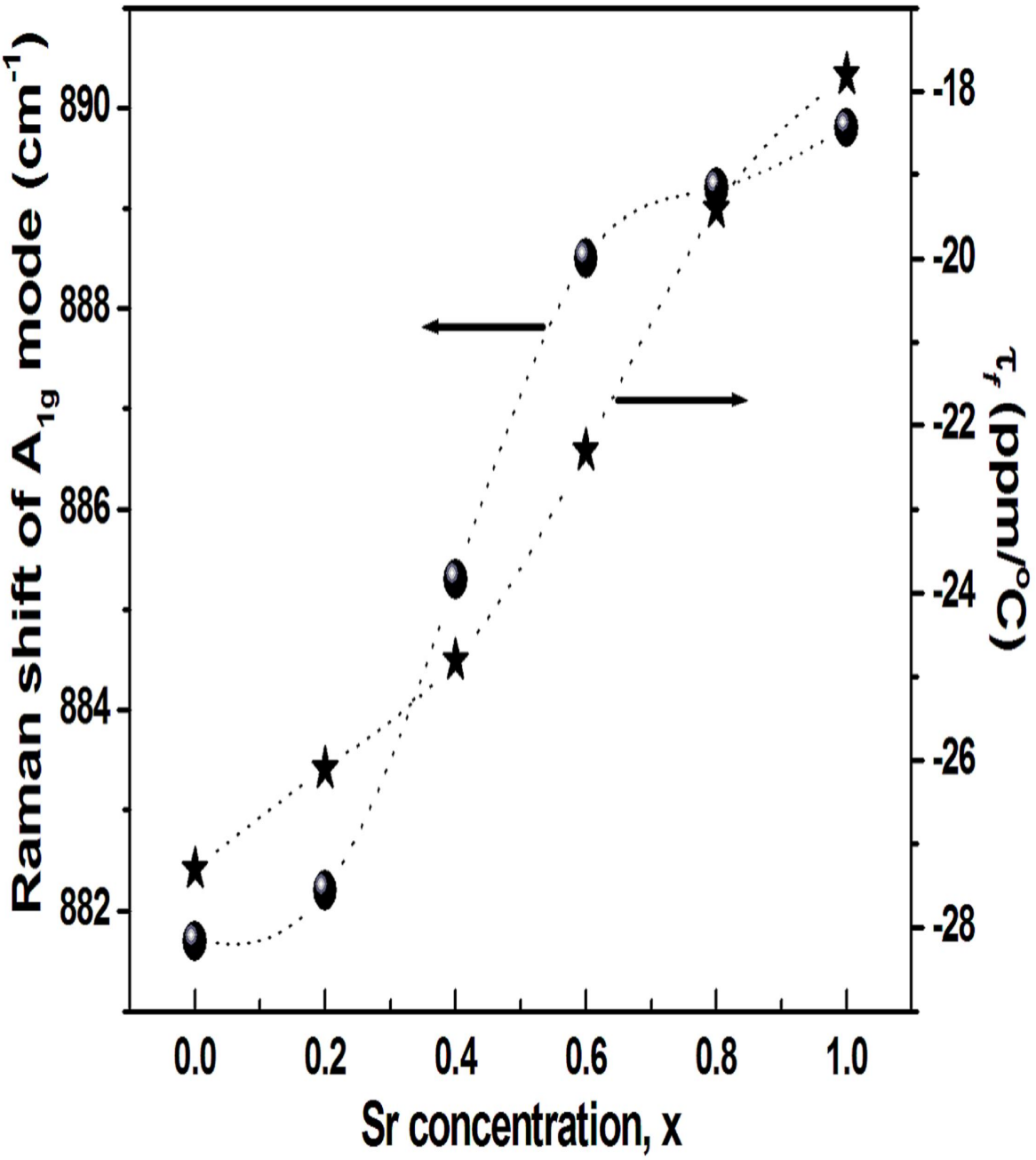

Fig. 11. Optical absorption spectra of $Ca_{1-x}Sr_xMoO_4$ compounds.

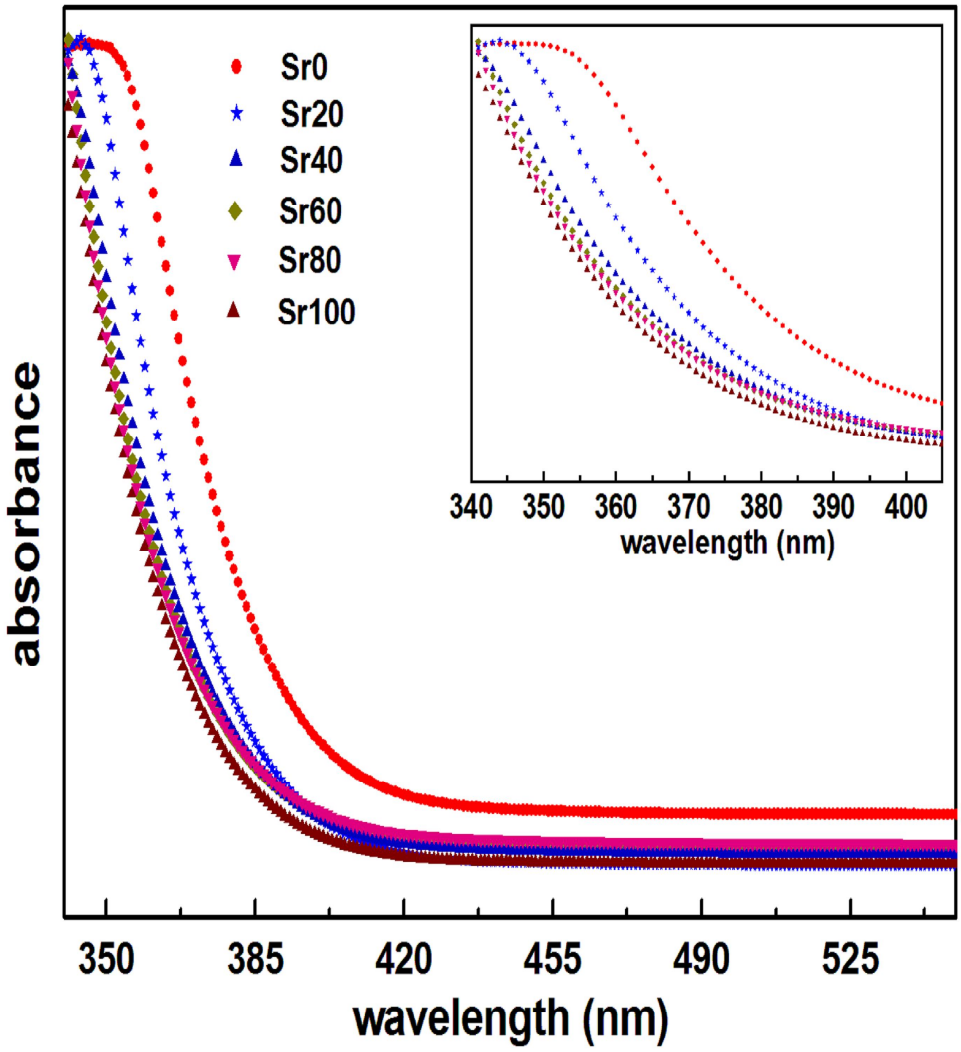

Fig. 12. Variation of band gap with Sr^{2+} concentrations.

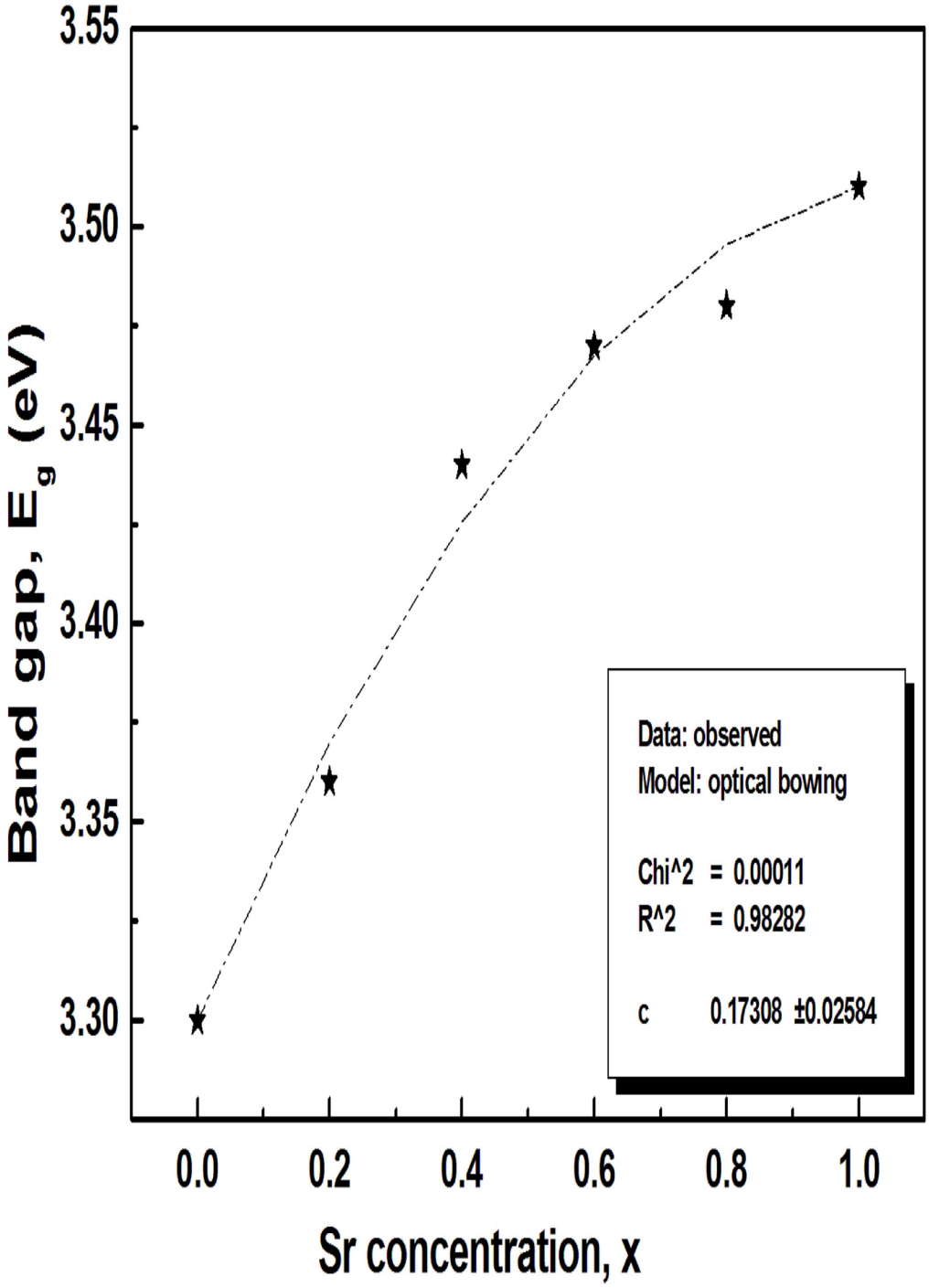

Table 1 Atomic positions, occupancies and thermal parameters of $Ca_{0.6}Sr_{0.4}MoO_4$ compound.

Atom	Wyckoff site	*x*	*y*	*z*	Occupancy	Uiso ($Å^2$)
Ca	4b	0(0)	0.25(0)	0.625(0)	0.6	0.0028
Sr	4b	0(0)	0.25(0)	0.625(0)	0.4	0.0036
Mo	4a	0(0)	0.25(0)	0.125(0)	1.0	0.0073
O	16f	0.2484(6)	0.1073(6)	0.0427(3)	1.0	0.0061

Table 2 Sintering temperature, density, porosity corrected dielectric constant and of $Ca_{1-x}Sr_xMoO_4$ compounds.

x	Sintering Temperature (^oC)	Theoretical density (ρ_{th})	Measured density (ρ_m)	Relative density (%)	ε_r
0	1200	4.249	4.083	96.1	9.65
0.2	1200	4.349	4.156	95.6	9.43
0.4	1200	4.442	4.298	96.8	9.32
0.6	1200	4.515	4.347	96.3	8.95
0.8	1200	4.608	4.385	95.2	8.53
1.0	1200	4.688	4.471	95.4	7.57

Table 3 Porosity corrected dielectric constant, molar volume, quality factor, Mo-O bond strength, temperature coefficient of resonant frequency and shift of A_{1g} mode of $Ca_{1-x}Sr_xMoO_4$ compounds.

x	ε_r	V_m ($Å^3$)	$Q \times f$ (GHz)	Mo-O bond strength (v.u)	τ_f (ppm/^oC)	Raman Shift of A_{1g} mode (cm^{-1})
0	9.65	78.17	51500	1.489	-27.3	881.7
0.2	9.43	80.02	39600	1.454	-26.1	882.2
0.4	9.32	81.91	35500	1.42	-24.8	885.3
0.6	8.95	84.01	38400	1.450	-22.3	888.5
0.8	8.53	85.72	46300	1.469	-19.4	889.2
1.0	7.57	87.66	48500	1.475	-17.8	889.8